Fabrication, Structural Characterization and Optical Properties of the Flower-Like ZnO Nanowires

L. Feng, A. Liu*, Y. Ma, M. Liu and B. Man
College of Physics and Electronics, Shandong Normal University, Jinan 250014, P.R. China

(Received January 10, 2010; in final form March 5, 2010)

Multipod flower-like zinc oxide (ZnO) nanowires have been successfully synthesized on Si(111) substrates using a pulsed laser deposition prepared Zn film as "self-catalyst" by the simple thermal evaporation oxidation of the metallic zinc powder at 850 ℃ without any other catalysts or additives. The pre-deposited Zn films by pulsed laser deposition on the substrates can promote the formation of the ZnO nuclei effectively. Also it can further advance the growth of the flower-like ZnO nanowires accordingly. X-ray diffraction, scanning electron microscope, high-resolution transmission electron microscopy, Fourier transform infrared spectrum, and photoluminescence were used to analyze the structure, morphology, composition and optical properties of the as-synthesized products. The results demonstrate that the nanowires were single crystalline with hexagonal wurzite structure, grown along the [0001] in the *c*-axis direction. Room temperature photoluminescence spectrum of the ZnO nanowires shows a nearband-edge ultraviolet emission (peak at $\approx$ 384 nm) and a deep-level green emission (peak at $\approx$ 513 nm). In addition, the growth mechanism of the flower-like ZnO nanowires is discussed in detail.

PACS numbers: 81.07.Bc, 81.05.Dz, 81.10.Aj

1. Introduction

In recent years, controlled synthesis of compound semiconductor nanostructures has attracted considerable interest in material fields, owing to that the properties of these materials depend mainly on their specific shapes, sizes and structures [1]. The interest in ZnO nanostructures is fueled and fanned by its prospects in optoelectronics applications because of its typical wide direct band gap (3.37 eV) with a large exciton binding energy (60 eV) at room temperature [2]. To date, the ZnO nanostructured materials, such as nanorods [3], nanotubes [4], nanowires [5], nanobelt [6] and nanobridge [7], have been successfully synthesized and have received much attention due to their novel physical properties and potential applications in nanodevices and nanosensors [8]. Such nanostructures would play an important role in understanding the role of dimensionality and size in optical [9], electrical [10], mechanical [11] and magnetic properties [12, 13]. Among them, the ZnO nanowires with a high surface-to-volume ratio have received particular attention and are expected to display significant properties. The ZnO nanowires have some obvious advantages over the ZnO bulk crystals and thin films due to the size confinement effects for the carriers and excitons [14]. Particularly, the stronger and more stable exciton effects at room temperature are very important in the light emission diodes (LED) and laser diodes (LD) [15, 16]. Moreover, the growth technologies of the ZnO nanowires are much simpler than that of the ZnO thin film. Therefore, various methods have been developed to fabricate the ZnO nanowires, for instance, chemical vapor deposition (CVD) [17], metal-organic chemical vapor deposition (MOCVD) [18], hydrothermal process [19], metal catalyzed vapor–liquid–solid process [20], aqueous solution method [21], pulsed laser deposition (PLD) [22], electrochemical deposition [23], microwave-assisted route [24], and ultrasonic spray pyrolysis [25]. However, catalysts usually have to be used in those methods during the synthesis of the ZnO nanowires The drawback is that the remains of the foreign catalyst in the products may influence some applications of the ZnO nanowires.

In this paper, we reported a simple synthesis method for the ZnO nanowires, which overcomes the drawbacks of previous methods. The flower-like ZnO nanowires were synthesized by simple thermal evaporating of high purity Zn powders onto a quartz tube at the temperature of 850 ℃ without introducing any external catalysts approach. Especially, in our experiment, a layer of Zn film is firstly pre-deposited on the Si(111) substrates by PLD before the thermal evaporating process. The PLD Zn film can promote the growth of the ZnO nanowires. The as-synthesized products are single-crystalline ZnO nanowires. This growth method allows a continuous synthesis and can produce ZnO nanowires with relatively

* corresponding author; e-mail: lah1120@gmail.com

high purity and low cost. Accordingly, it is probably useful for commercial-scale production. In addition, the possible growth mechanism and the optical property of the ZnO nanowires are also discussed in brief.

2. Experimental process

Firstly, Si(111) substrates were washed with absolute ethyl alcohol, and then ultrasonically cleaned in acetone, absolute ethyl alcohol, and deionized water for 30 min in sequence.

Secondly, a thin layer of Zn films was deposited on Si(111) substrates by PLD. The PLD apparatus and the experimental methods have been described in detail elsewhere [26]. High purity metal zinc (99.99%) with a diameter of 6 mm served as a target. The deposition chamber was evacuated by turbomolecular pump yielding typical base pressures of 3×10^{-4} Pa. The Q-switched Nd:YAG laser ($\lambda = 1064$ nm) was used to ablate the zinc target. The laser energy, the repetition rate, and the argon background pressure were set to be 100 mJ, 10 Hz, and 1.33 Pa, respectively. The substrates are Si(111) and the distance between the target and the substrates is 40 mm. For the Zn target ablated and thin film fabricated evenly, Zn target rotated clockwise and substrate rotated anticlockwise with a frequency of 7 rpm. The deposition time is 30 min and the growth temperature is 100 ℃. The film thickness was measured to be approximately 100 nm.

Finally, both the as-deposited Zn films by PLD and the high purity metallic Zn powder (99.99%) were inserted into the conventional horizontal quartz tube furnace (L4513II-2/QWZ) together. The Zn powder as the source material was placed in a high-temperature region of a quartz boat covered by another two-end open quartz cap. The Zn-coated Si(111) substrates prepared at the second step were placed in the low temperature region of the same boat. The distance between the Zn powder source and the Si substrate was about 10 mm. After heating the tube furnace to 850 ℃ at a rate of 50–100 ℃/min, the nitrogen gas with purity of 99.999% was introduced into the system with a flow of 200 sccm (standard cubic centimeters per minute) for 5 min to remove the residual air. Then the quartz boat loaded with the substrates and the source material were pushed into the center constant temperature region of the furnace. After the quartz boat was loaded into the furnace, a flow of mixture gas [O_2:Ar = 1:15 (by volume, 99.999% pure)] with the flow rate of 200 sccm was introduced to the system until the end of the reaction. The temperature of the Si substrate is about 700 ℃ in the system during the growth process. The reaction time was 20 min. After that, the reaction system was drawn out immediately and some white fluffy-like products were observed on the whole surface of the substrate. The products were collected for characterizations.

The morphology and structure properties of products were characterized and analyzed by X-ray diffraction (Rigaku D/max-rB Cu K_α, XRD), scanning electron microscopy (Hitachi S-570, SEM), high resolution transmission electron microscopy (JEOL JEM2100, HRTEM) and Fourier transform infrared spectrum (TENSOR27, FTIR). The room-temperature photoluminescence (PL) spectrum of the products was measured using Edinburgh Instruments FLS920 steady-state fluorescence spectrometer (U.K.) with Xe lamp as the excitation light source (with a wavelength of 325 nm).

3. Results and discussions

3.1. XRD analysis

The crystal structure of the as-synthesized products was characterized by XRD. Figure 1 shows a typical XRD pattern of the as-synthesized products. The results show that all the diffraction peaks in the pattern can be easily indexed as the pure hexagonal phase ZnO (wurtzite-type, space group: $P63mc$) with calculated lattice parameters of $a = 3.244$ Å, $c = 5.198$ Å, which is in good agreement with the reported standard values (JCPDS No. 36-1451). Compared with the standard diffraction patterns, no diffraction peaks of Zn or other impurities were observed in the spectrum, which indicates excellent crystal quality of the products. Furthermore, the clear and sharp peaks also revealed that the ZnO nanowires possess a high crystalline quality.

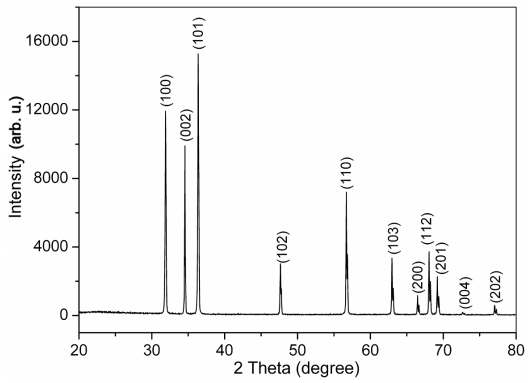

Fig. 1. X-ray diffraction pattern of the multipod flower-like ZnO nanowires synthesized at 850 ℃.

3.2. SEM analysis

Figure 2 reveals the representative SEM images of the as-synthesized products at different magnifications. Figure 2a, the panoramic morphology of the products, showed that the high yield accumulated ZnO nanowires were formed and distributed randomly on the substrate. It can be seen that most of the ZnO nanowires exhibited a radial multipod morphology having several legs and only a few tetrapod-like ZnO nanowires. From Fig. 2b and c it is clearly shown that the nanowires have a straight, smooth, pencil-like shape. The legs were connected to a junction which can be regarded as a central nucleus, forming a radial flower-like structure. The

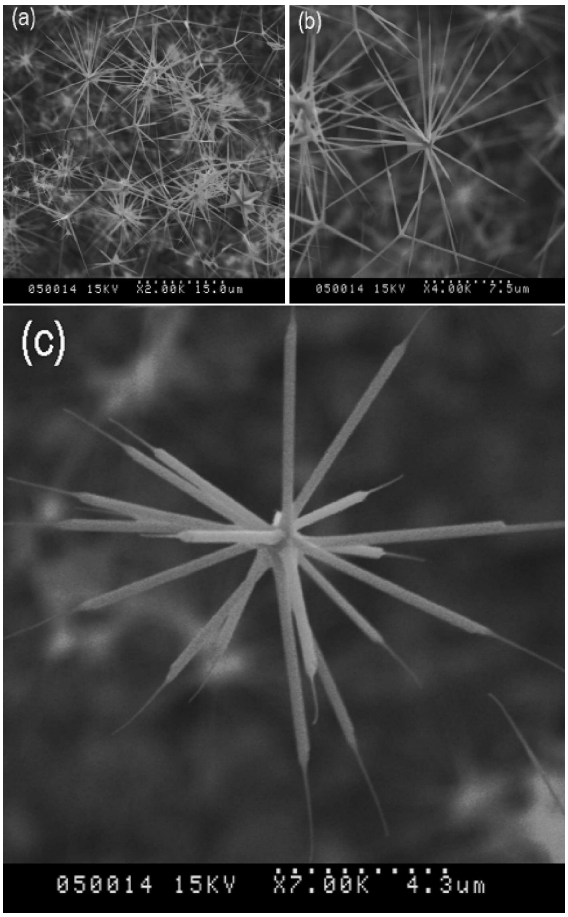

Fig. 2. Typical SEM images of the multipod flower-like ZnO nanowires at different magnifications: (a) 2000×, (b) 4000×, (c) 7000×.

central nucleus of the radial multipod flower-like ZnO nanowires is obviously bigger than those of the tetrapod nanowires. Most of the nanowires have a rod-like root and exhibit a sharp needle-like tip. The root diameters of the nanowires are in the range of 200–400 nm, while the tips have an average diameter about 40 nm. The length of the ZnO nanowires is about several micrometers. Furthermore, a small quantity of the ZnO lamellar crystal were also observed at some roots of the nanowires. Comparing the differences in the nucleus sizes, the essence of the legs of the tetrapod nanowires and those of the multipod nanowires are the same, which implies that they have the same growth mechanism [27]. The results indicate that the morphological differences between the tetrapod nanowires and the multipod nanowires might be a consequence of the difference in the size of the nucleus.

3.3. HRTEM analysis

To further understand the structural characteristics of the flower-like ZnO nanowires, HRTEM micrograph and selected area electron diffraction (SAED) pattern of the products were surveyed. Figure 3 shows the HRTEM images of the single ZnO nanowire, the visible lattice images illustrate that the nanowire is single-crystal in nature. The interplanar distance accurately measured is 0.26 nm, which corresponds to the distance between the two adjacent (0002) crystal planes of hexagonal ZnO. The (0002) planes are perpendicular to the growth direction of the ZnO nanowires, which confirms that the ZnO nanowires only grow along the *c*-axis direction. The inset in the upper-left-hand corner is the SAED pattern of single nanowire, which can be indexed to the diffraction of wurtzite ZnO crystal along the [0001] direction. Meanwhile, it also confirms that the as-synthesized ZnO nanowires are of single crystal structure.

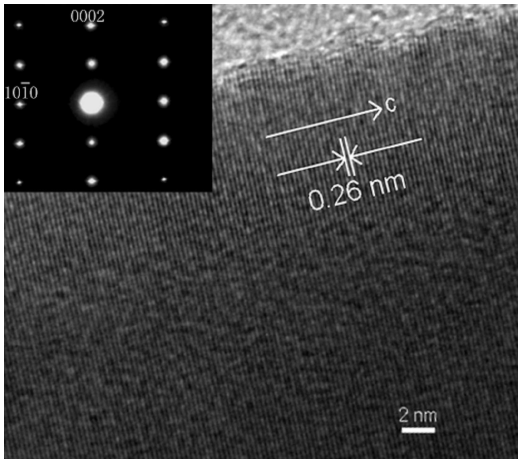

Fig. 3. HRTEM lattice image of the single ZnO nanowire. The upper-left-hand is the corresponding SAED image.

3.4. FTIR analysis

The products were mixed with potassium bromide (KBr) in the ratio of 1:100. The background spectrum recorded using KBr was subtracted from the products spectrum. Figure 4 exhibits FTIR spectrum of the ZnO nanowires. The absorption region from 400 to 2000 cm^{-1} generally represents the fingerprint region of the materials, which are unique in characteristics. The spectrum contains four prominent absorption bands. The band at 440.13 cm^{-1} corresponds to the asymmetric stretching mode of the as-synthesized wurtzite ZnO nanowires [28]. The absorption band around 548.46 cm^{-1} is the typical reference spectra of the pure ZnO powders often shown in [29]. The two bands at 1384.67 cm^{-1} and 1633.63 cm^{-1} are associated with Zn–O stretching vibration in wurtzite hexagonal-type ZnO crystal [30], which revealed that the products were hexagonal ZnO crystals. No other peaks observed in the spectrum confirms that the synthesized products are ZnO alone, which also correspond to the XRD.

3.5. Discussion of growth mechanism

According to the above analysis, we can infer the possible growth mechanism for the formation of the multipod

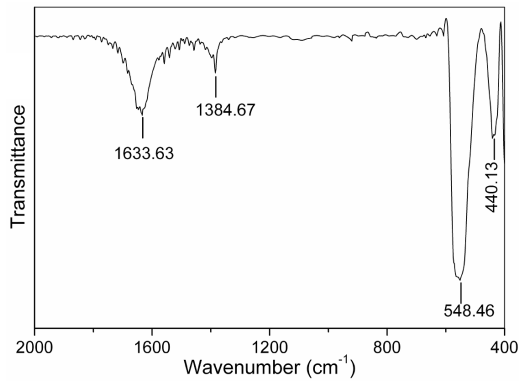

Fig. 4. FTIR spectrum of the multipod flower-like ZnO nanowires.

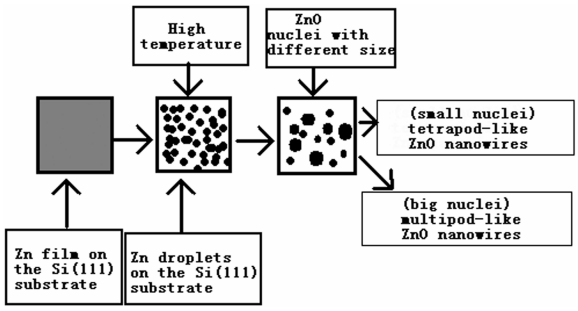

Fig. 5. Schematic illustration of the growth mechanism of the ZnO nanowires.

flower-like ZnO nanowires. The nanowires growth does not follow the conventional metal-catalytic VLS mechanism [31], but can be conceived as "self-catalyst" VLS growth mode [32]. The whole process is illustrated in Fig. 5. When the furnace temperature mounted into 850 ℃, much higher than the melting point of metallic zinc powder (the melting point of Zn = 419.5 ℃), the zinc vapors were produced from the source material. Because the amount of oxygen is deficient in our experiment, some suboxides (ZnO_x, $x < 1$) were also easily formed correspondingly. Due to the fact that Zn and Zn-suboxides (ZnO_x, $x < 1$) have a low melting temperature (approximately 419 ℃) [33], Zn and ZnO_x should be in vapor phases at the beginning of our experiment.

In the meantime, because the substrate temperature is higher than the melting point of Zn, the Zn films pre-deposited on the substrates are melted and aggregated to form the micro-sized Zn droplets on the substrate surface. Then, the oxygen react with the Zn droplets and form the ZnO nuclei on the substrate surface. Due to the flowing gas circulation, the Zn (g) or ZnO_x (g) vapor was transported by argon and condensed on the Si substrates located at a low temperature region. After that, the deposited Zn or ZnO_x also turned into liquid phase (l) Zn or ZnO_x (l, $x < 1$) droplets. These formed Zn or ZnO_x droplets migrated and merged with the original Zn droplets on the substrate surface, and then the incorporated droplets continued to absorb oxygen vapor around and formed more larger ZnO nuclei. So "self-catalyst" VLS growth has already begun to take effect during this initial growth period. The main reaction taking place in our experiment can be expressed as follows (g, l, s stand for gaseous, liquid, solid, respectively):

$$\mathrm{Zn(s)} \rightarrow \mathrm{Zn(g)}, \tag{1}$$

$$\mathrm{Zn(g)} + \mathrm{O_2(g)} \rightarrow \mathrm{ZnO}_x\mathrm{(g)}, \tag{2}$$

$$\mathrm{Zn(g)} \rightarrow \mathrm{Zn(l)}, \quad \mathrm{ZnO}_x\mathrm{(g)} \rightarrow \mathrm{ZnO}_x\mathrm{(l)}, \tag{3}$$

$$\mathrm{Zn(l)} + \mathrm{O_2(g)} \rightarrow \mathrm{ZnO(s)},$$

$$\mathrm{ZnO}_x\mathrm{(l)} + \mathrm{O_2(g)} \rightarrow \mathrm{ZnO(s)}. \tag{4}$$

In addition, the nucleation plays a key role in the growth of the flower-like ZnO nanowires in our experiment. According to the octa-twin nucleus model, ZnO nuclei formed in the atmosphere containing oxygen are octahedral nuclei [34]. The octahedral nuclei were considered to lead to the formation of the tetrapod nanowires [35]. Due to that the sizes of these aggregated ZnO nuclei were larger than the previously formed nuclei, the insufficiency of oxygen and the high temperature will make the accumulation of these aggregated nuclei to a multiple facets possible. It finally led to the formation of the polyhedral ZnO nuclei rather than octahedral nuclei. However, during this process, some small nuclei did not merge with other nuclei, which still kept the octahedron morphology and formed finally some tetrapod nanowires. It manifests that the formation of the multipod ZnO nanowires nuclei on the Zn-coated substrates is owing to the merging and growth of the polyhedral ZnO nuclei. Hence, the pre-deposited Zn films on the substrates can effectively promote the formation of the polyhedral ZnO nuclei. Those ZnO nuclei provide the energetically favored sites for the further growth of the multipod flower-like ZnO nanowires.

Furthermore, in the early stages of the reaction, it is probable that some ZnO nuclei or initially formed tiny single crystals are also easy to aggregate together under the driving forces of high surface energy, electrostatic force, and so forth [36]. Then each ZnO nucleus in the aggregate grows anisotropically along the *c*-axis. The aggregates finally become the flower-like nanowires assemblies. So, the obtained multipod ZnO nanowires are made up of several single crystals nanowires stretching radially from the center nuclei along *c*-axis directions. On the other hand, it is known that ZnO crystal has the wurtzite polar crystal structure which has a hexagonal unit cell with space group $P6mc$. The oxygen anions and Zn cations form a tetrahedral unit. The structure of the ZnO can be simply described as a number of alternating planes composed of tetrahedrally coordinated O^{2-} and Zn^{2+}, stacked alternatively along the *c*-axis.

Wurtzite structure model of the ZnO is shown in Fig. 6. As can be seen in Fig. 6, each Zn atom on the $\{10\bar{1}0\}$ prismatic faces parallel to the *c*-axis is two-coordinated Zn, whereas the Zn atom on the (0001) facet is one- or three-coordinated Zn. The inherent asymmetry along the

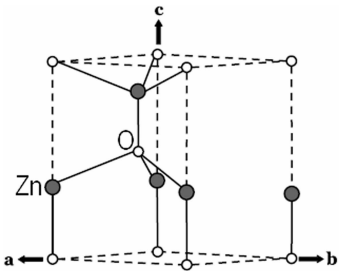

Fig. 6. Wurtzite structure model of the ZnO.

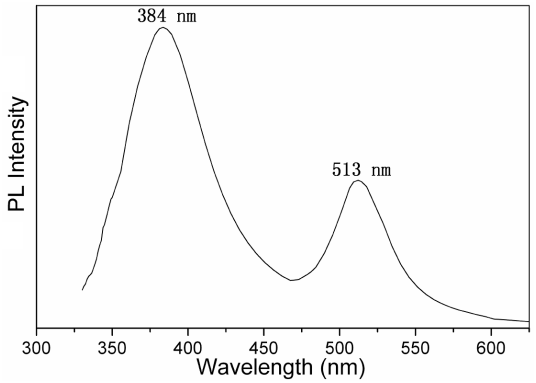

Fig. 7. Room temperature PL spectrum of the multipod flower-like ZnO nanowires.

c-axis leads to the anisotropic growth of the ZnO crystallites [37]. The formation of the multipod flower-like ZnO nanowires crystals is attributed to the difference in the growth rate of the various crystal facets. According to the lowest surface energy principle, the ZnO nuclei will be exposed at the crystal surfaces with the lowest energy [38]. Then the ZnO nanowires sprouted from these nuclei surfaces and grew along the [0001] direction because the surface energy of the (0002) facet is the lowest. According to the ZnO crystal growth mode, the growth rate along the [0001] direction is faster than along any other directions [39]. So, the growth along the [0001] direction is a dominating growth facet compared to other growth facets. Therefore, the multipod flower-like ZnO nanowires are finally formed. In our synthesized process, the multipod flower-like ZnO nanowires exhibited a preferential growth in the [0001] direction which also corresponded to the HRTEM and SAED patterns. In addition, the ZnO lamellar crystal is also observed at some roots of the nanowires due to the high temperature and the high super-saturation of the lateral growth.

3.6. PL spectrum analysis

Figure 7 shows the measurement of PL spectrum at room temperature of the products. The nanowires show two emission peaks, a strong ultraviolet (UV) band located at $\approx$ 384 nm, a green emission band centered at $\approx$ 513 nm. The UV emission originates from the excitonic recombination corresponding to the near band-edge emission of band gap ZnO. Moreover, the enhancement in UV emission intensity of the room temperature PL in our result was due to the improvement in the crystal quality of the flower-like ZnO nanorods.

Bagnall et al. [40] revealed that the improvement of crystal quality (decrease of impurities, and structure defects such as oxygen vacancies and zinc interstitials) can lead to a high near band-edge emission to deep-level emission ratio, resulting in the detectable UV emissions at room temperature. HRTEM image in Fig. 3 proved that the ZnO nanowires are single crystal structure with a low density of structural defects, an important factor for the observed UV emission at room temperature. Moreover, we observed a green light emission peak at $\approx$ 513 nm, commonly referred to a deep-level or trap-state emission. The green transition has been attributed to the single oxygen vacancy in the ZnO nanowires and the emission results from the radiative recombination of a photo-generated hole with an electron occupying of oxygen vacancy (V_O) [41]. At higher temperature the number of molten Zn atoms increases, combined with oxygen to form ZnO. To maintain the growth of nanostructures there should be a balance between the melting rate of Zn and the growth rate of ZnO. Since higher temperature requires more oxygen for the growth of nanostructures, then the constant flow rate of oxygen even at higher temperature will lead to oxygen deficiency. In our experiment, because the ZnO nanowires are fabricated at 850 ℃, a quantity of oxygen vacancies can also easily be produced. Thus, the green emission at $\approx$ 513 nm would be a result of the existence of the oxygen vacancies in the ZnO nanowires. Therefore, it is appropriate to conclude that there are a number of oxygen vacancies in the ZnO nanowires, and some defects could exist in the ZnO nuclei. Therefore, we expect that the ZnO nanowires with strengthened green light emission would be a promising material for applications in optoelectronic nanodevices.

4. Conclusions

In summary, the multipod flower-like ZnO nanowires were synthesized on Zn-coated Si(111) substrate through catalyst-free thermal evaporation in a tube furnace at 850 ℃. The pre-deposited Zn films by PLD on the substrate can promote the growth of the multipod flower-like ZnO nanowires effectively. The growth of the multipod flower-like ZnO nanowires mainly depends on the size of the formed ZnO nuclei. XRD, SEM and HRTEM show that the nanowires exhibited a single-crystalline wurtzite hexagonal structure and preferentially oriented in the [0001] direction. The growth mechanism of the multipod flower-like ZnO nanowires can be explained by a self-catalytic VLS growth model. Room temperature PL spectra of the ZnO nanowires show a strong UV emission band located at $\approx$ 384 nm and a green emission band centered at $\approx$ 513 nm, which was ascribed to the

near band-edge emission and the deep-level emission, respectively. We believe that the green-light emission property of the multipod flower-like ZnO nanowires may open up new opportunities for fabricating the optoelectronic nanodevices, such as LED and LD.

Acknowledgments

The authors are grateful for the financial support of the National Natural Science Foundation of China (10474059), the Provincial Natural Science Foundation of Shandong (Y2007 A05) and The Project-Sponsorship by SRF for ROCS, SEM, P.R. China.

References

[1] J.M. Jang, C.R. Kim, H. Ryu, M. Razeghi, W.G. Jung, *J. Alloys Comp.* **463**, 503 (2008).

[2] H. Xue, X.L. Xu, Y. Chen, G.H. Zhang, S.Y. Ma, *Appl. Surf. Sci.* **255**, 1806 (2008).

[3] S. Baruah, J. Dutta, *J. Cryst. Growth* **311**, 2459 (2009).

[4] L.G. Yu, G.M. Zhang, S.Q. Li, Z.H. Xie, D.Z. Guo, *J. Cryst. Growth* **299**, 184 (2007).

[5] D.S. Kim, U. Gösele, M. Zacharias, *J. Cryst. Growth* **311**, 3216 (2009).

[6] Z.L. Wang, *Mater. Sci. Eng. R* **64**, 33 (2009).

[7] J.S. Lee, M.S. Islam, S. Kim, *Nano Lett.* **6**, 1487 (2006).

[8] O. Lupan, G. Chai, L. Chow, *Microelectron. J.* **38**, 1211 (2007).

[9] A. Dakhlaoui, M. Jendoubi, L.S. Smiri, A. Kanaev, N. Jouini, *J. Cryst. Growth* **311**, 3989 (2009).

[10] S.W. Yoon, J.H. Seo, K.H. Kim, J.P. Ahn, T.Y. Seong, K.B. Lee, H. Kwon, *Thin Solid Films* **517**, 4003 (2009).

[11] B. Wen, J.E. Sader, J.J. Boland, *Phys. Rev. Lett.* **101**, 175502 (2008).

[12] G. Clavel, N. Pinna, D. Zitoun, *Phys. Status Solidi A* **204**, 118 (2007).

[13] S. Deka, P.A. Joy, *Solid State Commun.* **142**, 190 (2007).

[14] D. Stichtenoth, C. Ronning, T. Niermann, L. Wischmeier, T. Voss, C.J. Chien, P.C. Chang, *Nanotechnology* **18**, 435701 (2007).

[15] J. Bao, M.A. Zimmler, F. Capasso, X. Wang, Z.F. Ren, *Nano Lett.* **6**, 1719 (2006).

[16] E. Lai, W. Kim, P.D. Yang, *Nano Res.* **1**, 123 (2008).

[17] S.W. Kim, S. Fujita, H.K. Park, B. Yang, H.K. Kim, D.H. Yoon, *J. Cryst. Growth* **292**, 306 (2006).

[18] S.K. Mohanta, D.C. Kim, X.H. Zhang, C.B. Soh, A.M. Yong, H.K. Cho, S. Tripathy, *J. Cryst. Growth* **310**, 5312 (2008).

[19] S.K. Tzeng, M.H. Hon, I.C. Leu, *J. Cryst. Growth* **311**, 4510 (2009).

[20] S.Y. Li, C.Y. Lee, T.Y. Tseng, *J. Cryst. Growth* **247**, 357 (2003).

[21] M. Wang, C.H. Ye, Y. Zhang, H.X. Wang, X.Y. Zeng, L.D. Zhang, *J. Mater. Sci. Mater. Electron.* **19**, 211 (2008).

[22] Y.W. Song, S. Lee, S.Y. Lee, *J. Cryst. Growth* **310**, 4612 (2008).

[23] X.H. Wang, S. Liu, P. Chang, Y. Tang, *Phys. Lett. A* **372**, 2900 (2008).

[24] M.S. Mohajerani, M. Mazloumi, A. Lak, A. Kajbafvala, S. Zanganeh, S.K. Sadrnezhaad, *J. Cryst. Growth* **310**, 3621 (2008).

[25] M.T. Htay, Y. Hashimoto, N. Momose, K. Ito, *J. Cryst. Growth* **311**, 4499 (2009).

[26] M. Liu, X.Q. Wei, Z.G. Zhang, G. Sun, C.S. Chen, C.S. Xue, H.Z. Zhuang, B.Y. Man, *Appl. Surf. Sci.* **252**, 4321 (2006).

[27] X.M. Sun, X. Chen, Y.D. Li, *J. Cryst. Growth* **244**, 218 (2002).

[28] S. Rasouli, S.J. Moeen, A.M. Arabi, I. Tehran, *Prog. Color Colorants Coat.* **2**, 45 (2009).

[29] A. Matei, I. Cernica, O. Cadar, C. Roman, V. Schiopu, *Int. J. Mater. Form.* **1**, 767 (2008).

[30] M. Chang, X.L. Cao, H.B. Zeng, L.D. Zhang, *Chem. Phys. Lett.* **446**, 370 (2007).

[31] K.W. Kolasinski, *Curr. Opin. Solid State Mater. Sci.* **10**, 182 (2006).

[32] Q. Wan, K. Yu, T.H. Wang, C.L. Lin, *Appl. Phys. Lett.* **83**, 2253 (2003).

[33] Y.W. Heo, V. Varadarajan, M. Kaufman, K. Kim, D.P. Norton, F. Ren, P.H. Fleming, *Appl. Phys. Lett.* **81**, 3046 (2002).

[34] Y. Dai, Y. Zhang, Z.L. Wang, *Solid State Commun.* **126**, 629 (2003).

[35] M. Shiojiri, C. Kaito, *J. Cryst. Growth* **52**, 173 (1981).

[36] J. Xie, P. Li, Y.T. Li, Y.J. Wang, Y. Wei, *Mater. Chem. Phys.* **114**, 943 (2009).

[37] B.M. Wen, Y.Z. Huang, J.J. Boland, *J. Phys. Chem. C* **112**, 106 (2008).

[38] H. Iwanaga, M. Fujii, S. Takeuchi, *J. Cryst. Growth* **134**, 275 (1993).

[39] Q.J. Yu, W.Y. Fu, C.L. Yu, H.B. Yang, R.H. Wei, M.H. Li, S.K. Liu, Y.M. Sui, Z.L. Liu, M.X. Yuan, G.T. Zou, *J. Phys. Chem. C* **111**, 17521 (2007).

[40] D.M. Bagnall, Y.F. Chen, M.Y. Shen, Z. Zhu, T. Goto, T. Yao, *J. Cryst. Growth* **185**, 605 (1998).

[41] K. Vanheusden, W.L. Warren, C.H. Seager, D.R. Tallant, J.A. Voigt, B.E. Gnade, *J. Appl. Phys.* **79**, 7983 (1996).